Research Article

Synthesis, characterization and non-isothermal degradation kinetics of poly(ε-caprolactone)/Fe$_3$O$_4$-dye nanocomposites

R. Anbarasan[1] · V. Kohila[2] · B. Meenarathi[3] · G. Jeyalakshmi[4] · A. Jancirani[5]

Abstract

Congo red (CR) dye functionalized magnetic nanoparticle was synthesized and characterized by Fourier Transform Infra Red, UV–visible, fluorescence emission spectra, field emission scanning electron microscopy and vibrating sample magnetometry like analytical techniques. The prepared nanohybrid was chemically tagged with poly(ε-caprolactone) (PCL) via ring opening polymerization of ε-caprolactone. The PCL/Fe$_3$O$_4$–CR nanocomposites were characterized by the same techniques and differential scanning calorimetry and thermogravimetric analysis methods. The magnetic moment values of the Fe$_3$O$_4$ after the formation of the nanohybrid and nanocomposite were found to be reduced due to the encapsulation and surface functionalization effects. The magnetic moment value of Fe$_3$O$_4$ was decreased for the nanohybrid and nanohyrbid tagged PCL. The non-isothermal degradation kinetics was characterized in order to find out the energy of activation (E$_a$) for the thermal degradation of the PCL. For the sake of comparison, the non-isothermal degradation kinetics of the methylorange functionalized Fe$_3$O$_4$ end capped PCL was carried out and the results were critically compared.

1 Introduction

Poly(ε-caprolactone) (PCL) is a well known bio-medical candidate due to its bio-compatibility, bio-degradability, low cytotoxicity and low melting temperature (T$_m$). Generally, as we have described previously [1–3] PCL is synthesized through the ring opening polymerization (ROP) of CL in the presence of an initiator and a catalyst. In order to initiate the ROP of CL we used various functionalities, such as –OH, –NH$_2$, –CO$_2$H, –SO$_3$H, –SH, –CONH$_2$; among them the –OH group exhibited the highest yield. For instance, Oshimura and Takasu [4] reported the controlled ROP of CL in the presence of sulphonimide as a chemical initiator. Functionalized PCL was synthesized in the presence of stannous octoate (SO) as a catalyst [5]. In

2015, Hemmati et al. [6] synthesized PCL for bio-medical applications using propargyl alcohol as a chemical initiator. PCL was also synthesized in the presence of a cross linking agent and its enzymatic degradation studied [7]. Aminoacids initiated ROP of CL has also been reported in the literature [8]. Octadecanoic acid was used as an initiator for the ROP of CL [9]. Tributyltin alkoxides initiated ROP of CL was carried out and its non-isothermal degradation kinetics studied [10]. Microwave assisted methacrylic acid initiated ROP of CL was reported in the literature by Koopmans et al. [11]. The graphene oxide nanosheet initiated ROP of CL was reported by Wang and his research team [12]. Samarium acetate as a chemical initiator for the ROP of CL has been reported in the literature [13]. Benzyl alcohol [14] and luminol [15] were also used for

✉ R. Anbarasan, anbu_may3@yahoo.co.in | [1]Department of Chemical Engineering, National Taiwan University, Taipei 10617, Taiwan. [2]Department of Chemistry, KCET, Virudhunagar, Tamilnadu 626 001, India. [3]Department of Polymer Technology, KCET, Virudhunagar, Tamilnadu 626 001, India. [4]Department of Chemistry, SFR College for Women, Sivakasi, Tamilnadu, India. [5]Department of Chemistry, The American College, Madurai, Tamilnadu, India.

the ROP of CL. Meenarathi et al. [16] used near infrared dye grafted MWCNT system, Fe_3O_4/acidfuchsin dye [17], Ag/acidfuchsin dye [18], bromophenol blue dye [19] and Fe_3O_4/alizarinred dye [20] initiators for the ROP of CL. However, despite a thorough literature survey, we could not find any report describing a non-isothermal degradation kinetics study of magnetic and fluorescent PCL. Because of their potential usage for various bio-medical purposes this leads the authors to do the present investigation.

Since PCL is used in the bio-medical engineering field it is necessary to find out its thermal properties, particularly its thermal degradation behavior. The non-isothermal degradation kinetics of PCL based triblock copolymer was reported within the last year [21]. In addition the thermal degradation kinetics of blends of poly(trimethylene carbonate) with PCL was studied by Marquez et al. [22]. Aoyagi et al. [23] reported the degradation kinetics of PCL and its blend with PLLA and poly(hydroxybutyrate). Su et al. [24] published their results on the degradation kinetics of PCL with the Ea value of 70 kJ/mol. Sivalingam et al. [25] also studied the thermal degradation kinetics of PCL. Our literature survey indicated that there have been no research publications are available on the degradation kinetics of PCL/Fe_3O_4–CR nanocomposite system. The novelty of the present investigation is the study of the influence of the chemical structure of two dyes methyl orange (MO) and CR on the thermal degradation behavior of PCL. The chemical structure of dye plays a vital role on the thermal degradation behavior of PCL. The MO contains one tertiary amino group, one azo group and one –SO_3Na group whereas the CR contains two azo groups, two amino groups and two –SO_3Na groups. Hence, the chemical structure of dye can influence the thermal degradation behavior of PCL. Apart from their fluorescent nature, they can initiate the ROP of CL. For these reasons it is necessary to study the influence of chemical structure of dyes on the thermal and spectral behavior of PCL. The main aim of the present investigation is to study the influence of chemical structure of dyes on the thermal degradation behavior of PCL.

2 Experimental

2.1 Materials

Ferric chloride ($FeCl_3$), ferrous sulphate ($FeSO_4$), sodium hydroxide (NaOH), methyl orange (MO) and congo red (CR) dye were purchased from Nice Chemicals private limited, India. Double distilled water (DDW) was used for making solutions. ε-caprolactone (CL, monomer) and stannous octoate (SO, catalyst) were purchased from Sigma Aldrich company limited, USA and used as-received. Chloroform

and diethyl ether were purchased from Spectrum Chemicals private limited, India.

2.2 Synthesis of CR functionalized Fe_3O_4

10 g $FeCl_3$ and 5 g $FeSO_4$ each were dissolved in 100 mL DDW separately; then the two solutions were mixed at room temperature under vigorous stirring conditions. After the vigorous stirring for 5 min, a NaOH solution was added drop by drop (10 g NaOH dissolved in 100 mL DDW) till the attainment of a strongly alkaline pH (ca 12.5). The addition process was continued after the alkaline pH for the next 2 h. The Fe_3O_4 formation was confirmed by the appearance of a dark colored precipitate (Scheme 1) [26, 27]. At the end of reaction the reactants were transferred to a 500 mL beaker and put on a magnetic bar and kept for 5 min. The black colored precipitate settled down and the remaining supernatant solutions were pipetted out. 50 mL of fresh DDW was added to the Fe_3O_4 nanocrystals, stirred well and kept on the magnetic bar for 5 min. In the same way the process of purification was continued 3
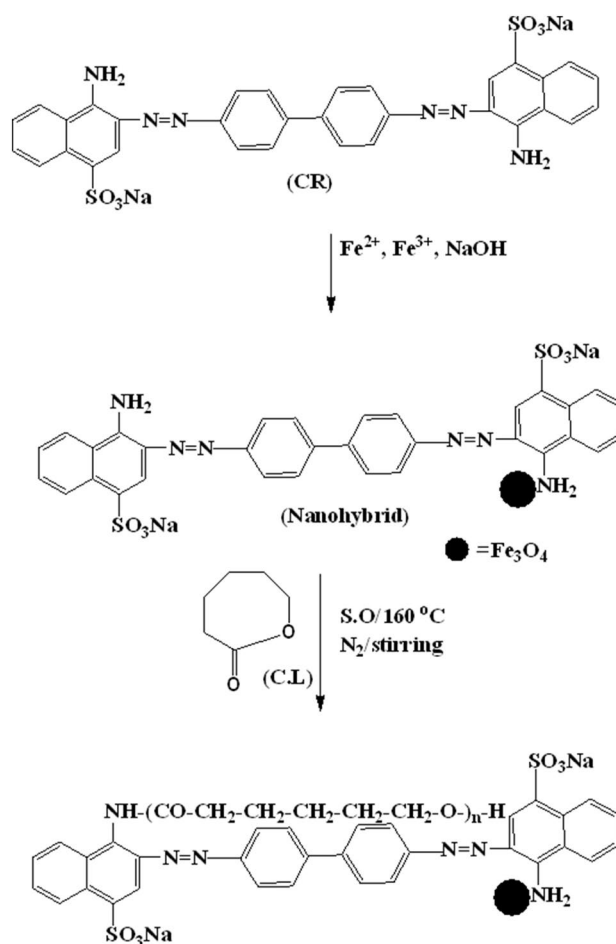
Scheme 1 Synthesis of Fe_3O_4–CR end capped PCL

times. The excess NaOH, $FeSO_4$ and $FeCl_3$ were removed by the repeated washing and the precipitate dried at 110 °C for 8 h. The thus obtained fine black powder is known as Ferrite (Fe_3O_4). The thus obtained Fe_3O_4 nanocrystals were ground and stored in a zipper lock polyethylene bag. In the case of CR or MO dye functionalized Fe_3O_4 synthesis, the above said procedure was followed in the presence of 5 g of CR or MO dye powder in 100 mL DDW without adding NaOH. The end product then was a dark brown powder the CR functionalized Fe_3O_4 nanohybrid system [18]. A similar procedure was repeated for the preparation of Fe_3O_4/MO nanohybrid system.

2.3 Synthesis of poly(ε-caprolactone)/Fe_3O_4–CR nanocomposite

1 g CL monomer was accurately weighed in a 25 mL capacity round bottomed flask (RBF). 0.001 g of SO catalyst was added into the RBF. 0.015 g of Fe_3O_4–CR or Fe_3O_4–MO nanohybrid initiator was accurately weighed and mixed with the RBF. The ROP of the CL was carried out at five different mass loadings [M] of CL 0.5, 1.0, 1.5, 2.0 and 2.5 g. Here the ratio between the monomer and catalyst, [M/C] was maintained at 1000. After the physical mixing, the RBF was kept in an oil bath at 160 °C and heated under N_2 atmosphere for 2 h (Scheme 1). During the course of the reaction the color of the Fe_3O_4–CR changed and it became a highly viscous mass [18]. Even though, the ROP of the CL was carried out by a bulk polymerization method, it was further purified by a re-precipitation method. The highly viscous mass was dissolved in 25 mL chloroform and re-precipitated by the addition of 250 mL of diethyl ether. The total content was transferred into a 500 mL beaker and evaporated to dryness under fume hood for overnight. After the evaporation and the aerial drying process, a dark brown color product was obtained. This was again weighed and stored in a zipper lock bag and named as Fe_3O_4/CR end capped PCL. The mechanism behind the initiation of ROP of CL can be explained on the basis of co-ordination insertion mechanism. In the present investigation, SO was used as a catalyst for the ROP of CL and this co-ordinated with the –NH_2 group of Fe_3O_4/CR nanohybrid system in the first step. The ROP of CL was carried out at 160 °C under N_2 atmosphere for 2 h. Now this nanohybrid is acting as a heterogeneous initiation system because the added initiator is not completely soluble in CL monomer due to difference in melting and boiling points. In the second step, the co-ordinated nanohybrid is interacted with the CL through –C–O–C linkage. In such a way the ring structure of CL was opened and one hydrogen atom from the –NH_2 group of nanohybrid was transferred to the PCL chain end. Finally, it produced the PCL/Fe_3O_4–CR

nanocomposite system. A similar mechanism was followed by the PCL/Fe_3O_4–MO system.

2.4 Characterization techniques

The UV–visible spectrum was measured by dissolving the sample in $CHCl_3$ solvent. The instrument used here was a 3600 NIR spectrophotometer, (Shimadzu Corporation, Japan) from 200 to 800 nm. The same sample solution was subjected to fluorescence emission measurement from 350 to 700 nm by using a SL174 (Elico Analytical Instruments, India) instrument. The FTIR spectrum was recorded with the help of a 8400 S (Shimadzu Corporation, Japan) model instrument by a KBr pelletization method from 400 to 4000 cm^{-1}. 3 mg polymer was ground with 200 mg of spectral grade KBr and made into a disc under the pressure of 7 tons. Field emission scanning electron microscopy (FESEM) (better resolution at higher magnification in the whole range of accelerating voltages even for beam sensitive specimens are the advantages of FESEM over SEM) was used to examine the morphological behaviour of the polymer with the help of S4800 (FESEM-Hitachi Japan) instrument. The % compositions of the elements present in the PCL were determined by electron dispersive energy (EDX, thermal source). The surface morphology of the samples were characterized by JSM 6300, JEOL product, SEM, USA instrument. The PCL semi-crystalline powder sample was subjected to gold coating under vacuum for 15 min followed by SEM imaging. The melting temperatures (T_m) of the polymer samples were determined by using a Thermal Analyst 2000 Differential Scanning Calorimeter 910S, (Dupont, USA) model instrument. All the measurements were done under N_2 atmosphere in a temperature range of RT to 100 °C with 10 °C/min heating rate. Thermal stabilities of the polymer samples were measured by 951 thermogravimetric analyzer (Dupont, USA). Thermograms were recorded under an air atmosphere in a temperature range of 30–800 °C at five different heating rates 5, 10, 15, 20 and 25 °C/min. X-ray diffraction was carried out using an advanced scanning instrument from 2θ value of 2°–60° at the scanning rate of 2°/min (XRD, BrukerXS08 model instrument). Molecular weight of the polymer samples were carried out using gel permeation chromatography (GPC), (Perkin Elmer Series 200) (USA) in THF solvent and poly(styrene) as an internal standard.

From the FTIR spectrum the relative intensities were calculated, from which the order of reaction was determined using Eq. (1),

$$\text{FTIR-RI of } [C{=}O/C{-}H] = A_{1726}/A_{730} \qquad (1)$$

where A_{1726} is the corrected peak area of a peak at 1726 cm^{-1} and A_{730} is the corrected peak area at 730 cm^{-1}.

The rate of polymerization (Rp) was calculated from the absorption value of UV–visible spectra and fluorescence emission intensity value of fluorescence emission spectra, as given in Eq. (2).

$$\text{Rate of polymerization (Rp)} = \frac{\text{Abs. (or) FEI}}{V t M.W} \times 1000 \qquad (2)$$

where V, is total volume of the reactants; t, reaction time in seconds; M.W, molecular weight of CL, monomer.

3 Results and discussion

The results and discussion part of the present investigation is subdivided into four parts namely, (1) characterization of Fe_3O_4–CR nanohybrids, (2) characterization of PCL/Fe_3O_4–CR nanocomposites, (3) non-isothermal degradation kinetics of the PCL/Fe_3O_4–CR nanocomposite system, (4) non-isothermal degradation kinetics of the PCL/Fe_3O_4–MO nanocomposite system.

3.1 Characterization of the Fe_3O_4–CR nanohybrid system

3.1.1 FTIR study

Characterization results for the above synthesized Fe_3O_4–CR nanohybrid system are shown in Fig. 1 as characterized by various analytical techniques; FTIR, UV–visible, FES, VSM and FESEM. The FTIR spectrum of the pristine Fe_3O_4 is shown in Fig. 1a. The broad –OH stretching appearing at 3400 cm^{-1} is due to the hydroxyl stretching vibrations of the intercalated water molecules. A twin peak appeared at 576 and 619 cm^{-1} corresponded to the metal oxide (M–O) stretching vibration of Fe_3O_4. This is in accordance with an earlier report from our research team [26].
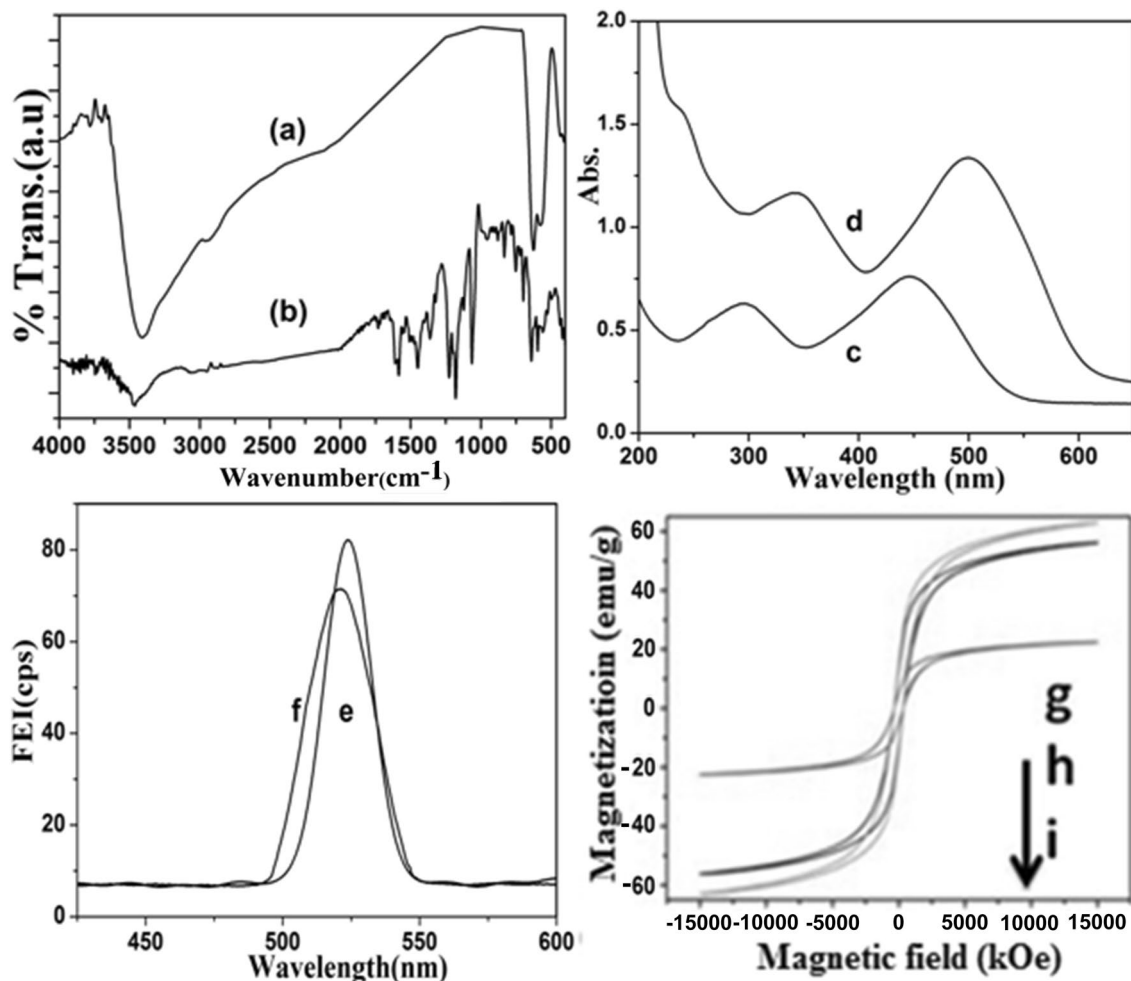

Fig. 1 FTIR spectrum of **a** Fe_3O_4, **b** Fe_3O_4–CR nanohybrid, UV–visible spectrum of **c** CR, **d** Fe_3O_4–CR nanohybrid, Fluorescence emission spectrum of **e** CR, **f** Fe_3O_4–CR nanohybrid, VSM loops of **g** Fe_3O_4, **h** Fe_3O_4–CR nanohybrid, **i** PCL/Fe_3O_4–CR nanocomposite system

Figure 1b is ascribed to the FTIR spectrum of Fe_3O_4–CR nanohybrid system. Here also one can see the –OH and M–O stretching bands corresponding to the Fe_3O_4–CR nanohybrid system. A small peak appeared at 1727 cm^{-1} is due to the C=O stretching of a carbonate. The C–N stretching of the CR dye was observed at 1359 cm^{-1} and the aromatic bending vibrations of CR dye appeared at 699, 753 and 839 cm^{-1} [1, 28]. The $–SO_2$ and $–SO_3–Na^+$ stretchings [18] of CR appeared at 1070, 1166 and 1231 cm^{-1} respectively. A sharp peak at 1450 cm^{-1} can be explained on the basis of N=N structure of CR dye. The p-disubstituted benzenoid structure of CR dye was observed at 1590 cm^{-1}. Thus, the appearance of new peaks confirmed the existence of strong interactions between the CR dye and Fe_3O_4 through the amino groups of the CR. Hence, the FTIR spectrum confirmed the functional groups present in the Fe_3O_4–CR nanohybrid system.

3.1.2 UV–visible study

Figure 1c, d represent the UV–visible spectrum of CR before and after the nanohybrid formation, respectively. The UV–visible spectrum of CR (Fig. 1c) exhibited two peaks, at 446 nm (corresponding to the monomeric form of CR dye) and 292.8 nm (corresponding to the dimeric form of CR dye). Recently, we reported [29] the UV–visible spectrum of CR dye before and after chemical grafting reaction. The nanohybrid (Fig. 1d) again exhibited two peaks (499.2 and 343.2 nm), corresponding to the monomeric and dimeric structures of CR with red shifting. The red shift by 53 nm is attributed to the existence of chemical interaction between Fe_3O_4 and the amino groups of the CR dye. If the $–SO_3Na$ group of the CR dye interacts with the Fe_3O_4 surface automatically the structure of Fe_3O_4 will be degraded due to the very high acidic pH and more electronegativity nature.

3.1.3 Fluorescence spectroscopy study

The advantage of using dye moieties (as a fluorescence probe in bio-medical engineering field) is its fluorescence activity. The CR dye has fluorescence property even after the nanohybrid formation with Fe_3O_4 and nanocomposite formation with PCL. Hence it is necessary to study the fluorescence property with the help of fluorescence emission spectrum measured under quantitative conditions. Figure 1e indicates the fluorescence emission spectrum of pure CR dye at the wavelength of 523 nm. After the nanohybrid formation the emission peak was blue shifted to 520.7 nm (Fig. 1f) due to the decrease in crystal size [29]. This can be explained as follows: the size of the Fe_3O_4 crystals was reduced due to the surface functionalization

by CR dye. As a result of an increase in Surface Plasmon Resonance (SPR) effect, the electronic clouds on ferrite were extended to the CR dye. Such an electronic cloud will reduce the crystal size of the Fe_3O_4. The reduction in size of the Fe_3O_4 crystal is further supported by FESEM analysis.

3.1.4 VSM study

The first and foremost characterization technique for magnetic material is the VSM technique. Figure 1g, h indicate the VSM loops of pristine Fe_3O_4 and its nanohybrid, respectively. Before the surface functionalization reaction, the Fe_3O_4 exhibited a magnetic moment value of 62.0 emu/g. For the same Fe_3O_4 after the structural modification with CR dye, the VSM value was suppressed to 55.1 emu/g. The decrease in VSM value confirmed the existence of chemical interactions between Fe_3O_4 surface and CR dye molecules. We noted a similar observation [26] due to the surface functionalization and encapsulation effects offered by a drug molecule towards ferrite. Figure 1i shows the VSM loop of the PCL/Fe_3O_4–CR nanocomposite system; it will be discussed in the following sections.

3.1.5 FESEM study

Figure 2a shows the FESEM image of the nano Fe_3O_4, with spherical and rod shapes. The sizes of the sphere were calculated as approximately 100 nm. The important point noted here is the synthesis of ferrite under strongly alkaline condition leads to the formation of different size and shape (non homogeneity) particles. Figure 2b indicates the FESEM image of the Fe_3O_4–CR nanohybrid system. The preparation procedure is mentioned in the experimental part. It was found that the size of the Fe_3O_4 nanoparticles were reduced or compressed. The average size of the Fe_3O_4 nanoparticles was determined as 22 nm. The decrease in particle size with homogeneity confirmed the existence of chemical interaction between Fe_3O_4 and CR dye. Figure 2b also shows a nanosquare and nanocube. This must have been formed due to the agglomerisation of nanorods under the influence of the CR dye. From the FESEM analysis we concluded that after the nanohybrid formation the size of the Fe_3O_4 could be reduced as we also showed previously [18, 26].

3.1.6 XPS study

The interaction between Fe_3O_4 and CR dye were confirmed by XPS. Figure 2c indicates the XPS of pristine Fe_3O_4. The spectrum showed peaks corresponding to O1s (532.2 eV), Fe2$p_{3/2}$ (712.7 eV), Fe2$p_{1/2}$ (716.5 eV) and Fe3p (54.2 eV).
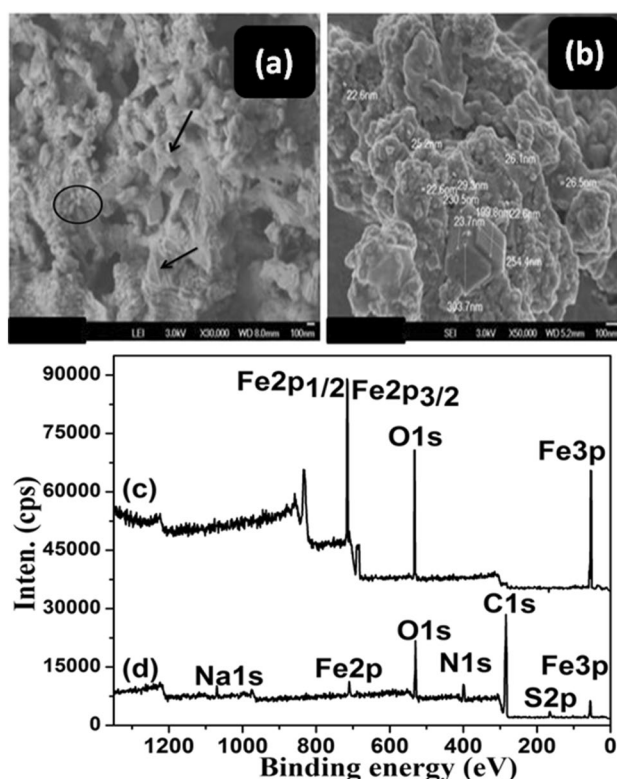
Fig. 2 FESEM image of **a** Fe_3O_4 and **b** Fe_3O_4–CR nanohybrid, XPS of **c** Fe_3O_4 and **d** Fe_3O_4/CR nanohybrid system

Figure 2d represents the XPS of Fe_3O_4/CR nanohybrid system. Here also one can observe the above mentioned peaks with some new peaks such as S2p (164.1 eV), C1s (286.7 eV), N1s (397.3 eV) and Na1s (1067.4 eV) due to the added CR dye. Thus the XPS confirmed the nanohybrid formation between Fe_3O_4 and CR dye.

3.2 Characterization of poly(ε-caprolactone)/ Fe_3O_4–CR nanocomposite

3.2.1 FTIR study

The second part of the present investigation was the characterization of the PCL/Fe_3O_4–CR nanocomposite system. Here the [M] was varied 0.5, 1.0, 1.5, 2.0 and 2.5 g and followed the bulk polymerization technique. The FTIR spectra are shown in Fig. 3a–e. The metal oxide stretching vibration was observed at 446 cm^{-1}. The C–H out of plane bending vibration was observed at 738 cm^{-1}. The ester C–O–C linkage was observed at 1179 cm^{-1}. The C–N stretching of CR dye was observed at 1373 cm^{-1}. The ester carbonyl group of PCL is noted at 1723 cm^{-1} [30, 31]. The aliphatic C–H stretchings are noted at 2859 and 2949 cm^{-1} corresponding to the C–H symmetric and anti-symmetric stretching of PCL, respectively. The –OH stretching can be seen at 3440 cm^{-1}. Peak at 1039 and 1113 cm^{-1} are associated with the –SO_2 stretching of CR dye. Thus the FTIR spectrum confirmed the functional groups expected to be present in both PCL and the Fe_3O_4–CR nanohybrid system. The important point noted here is that while increasing the [CL] from 0.5 to 2.5 g, the corrected peak areas of the carbonyl stretching (1723 cm^{-1}) and C–H out of plane (738 cm^{-1}) bending vibrations were increased in a linear manner. In order to find out the order of the reaction, the plot of log [M] versus log($RI_{[C=O/C–H]}$) was drawn (Fig. 3f). The plot showed an increasing trend with the slope value of 0.18. This indicated that 0.18 mol of CL was required to form one mole of PCL. The kinetic study indicated that Fe_3O_4–CR nanohybrid system was an effective initiator towards the ROP of CL. Our result is in accordance with our earlier report [20]. During the polymerization process, the cyclic structure of CL underwent ring opening process
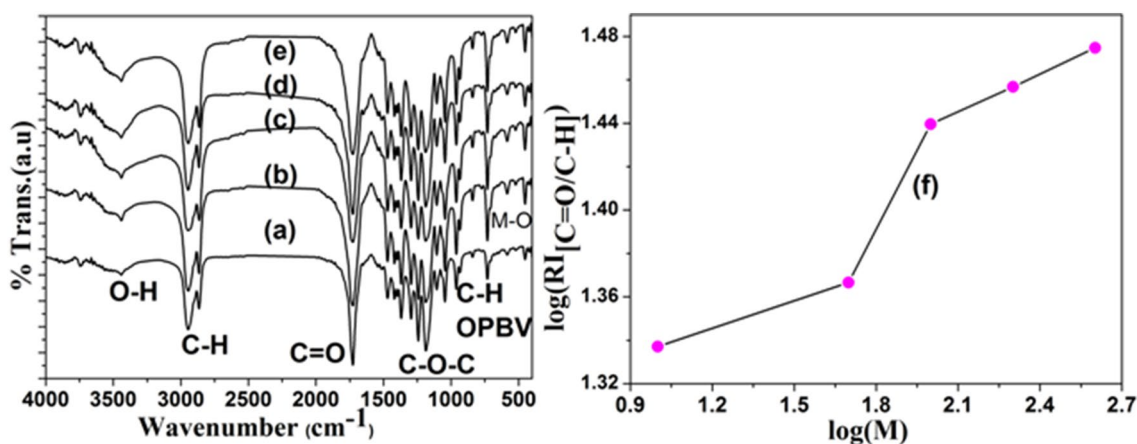

Fig. 3 FTIR spectrum of PCL/Fe_3O_4–CR nanocomposite synthesized at [M] of **a** 0.50 g, **b** 1.5 g, **c** 2.0 g, **d** 2.5 g, **e** 3.0 g and **f** plot of log[M] versus log($RI_{[C=O/CH]}$)
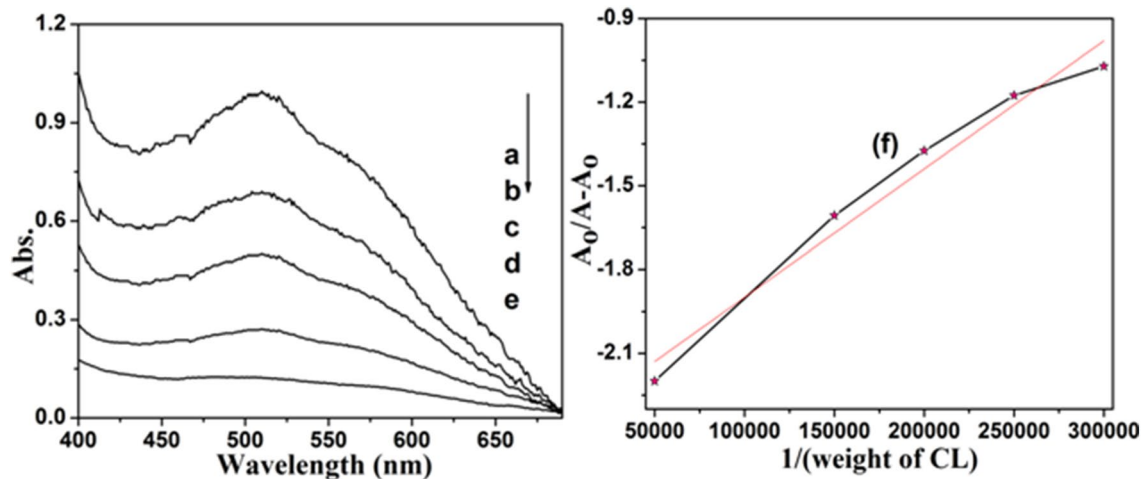
Fig. 4 UV-visible spectrum of PCL/Fe$_3$O$_4$–CR nanocomposite synthesized with [M] of **a** 0.50 g, **b** 1.0 g, **c** 1.5 g, **d** 2.0 g, **e** 2.5 g and **f** plot of A$_o$/[A − A$_o$] versus 1/[M]

and attached one by one through co-ordination insertion mechanism. While increasing the concentration of CL, the number of repeating units added with the polymer chain is increased. In order to find out the role of CL monomer during the course of the reaction, the above said kinetic plot was made. The rate at which the ring structure of CL was opened in the presence of fixed concentration of initiator, catalyst, time and temperature and added with each other, lead to the polymer formation. The present investigation followed the 0.18 order of reaction with respect to CL concentration.

3.2.2 UV–visible spectroscopy study

Figure 4 indicates the UV–visible spectra of the PCL/Fe$_3$O$_4$–CR nanocomposite system. The monomer concentration was varied from 0.5 to 2.5 g. It was found that while increasing the [M], the absorbance values were correspondingly decreased (Fig. 4a–e). This is due to the decrease in number of initiator species [18]. The number of initiator species per unit area is reduced while increasing the concentration of CL monomer. In order to find out the binding constant, the plot of (1/weight of CL) versus A$_0$/A − A$_0$ (Fig. 4f) was drawn and the plot was found to be nearly a linear line. The binding constant value was determined from the ratio of the intercept and slope value of the plot as 5.13×10^5 [M]$^{-1}$. When compared with our prior report [18] the present system yielded a good binding constant value. This can be explained on the basis of chemical structure of an initiator species.

3.2.3 FES of PCL/Fe$_3$O$_4$–CR nanocomposite

The binding constant and number of binding sites were determined from the fluorescence emission spectrum of PCL/Fe$_3$O$_4$–CR nanocomposite synthesized at various monomer concentrations. While increasing the monomer concentration from 0.5 to 2.5 g the fluorescence emission intensity (FEI) was found to be decreased (Fig. 5a–e). This is due to the decrease of initiator concentration for the ROP of CL. From the emission intensity value one can find out the order of ROP reaction by plotting log (weight of CL) versus log Rp (Fig. 5f). The plot was found to be nearly a straight line with decreasing trend. It means while increasing the CL concentration, the fluorescence emission intensity was decreased. The order of reaction was determined as 0.31. This indicated that 0.31 g of monomer was required to form one mole of PCL (based on FEI value). From the fluorescence emission spectrum it was also possible to find out the number of binding sites and binding constant for CR dye with PCL. The binding constant and the number of binding sites were determined from the plot of log(weight of CL) versus log(I$_0$ − I/I) (Fig. 5g). The plot showed a straight line with the slope value of 1.21 and the intercept value of 3.01 (determined by linear fit method). The slope value gives the binding constant whereas the intercept value gives the number of binding sites. In case of CR, we have two amino groups and two –SO$_3$Na groups. During the course of the reaction the –SO$_3$Na group may be converted to a –SO$_3$H group. One amino group is bonded with the Fe$_3$O$_4$. The remaining three functional groups (1-amino group and 2-SO$_3$H groups) might be involved in the ROP of CL [18]. Again this confirmed the existence of chemical interaction between CR dye and PCL chains.
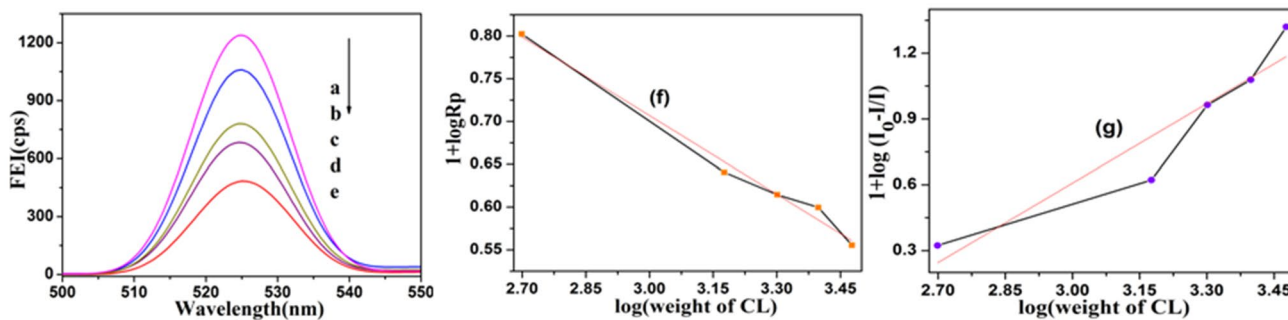
Fig. 5 Fluorescence emission spectra of PCL/Fe$_3$O$_4$–CR nanocomposite synthesized at [M] of **a** 0.50 g, **b** 1.5 g, **c** 2.0 g, **d** 2.5 g, **e** 3.0 g, **f** plot of log(weight of monomer) versus log Rp and **g** plot of log(weight of monomer) versus log[I$_o$ − I/I]

The number of binding sites exactly matches with the structure.

3.2.4 DSC study

The melting temperature (T$_m$) of PCL synthesized at five different heating rates was determined by DSC. The DSC thermogram exhibits one endothermic peak at 65 °C due to the melting of PCL (Fig. 6a–e). It was very interesting to note that while increasing the heating rate, the T$_m$ value of PCL was increased linearly. While increasing the heating rate between 5 and 25 °C/min, the T$_m$ value was varied between 64.4 and 68.4 °C. This can be explained on the basis of fast scanning of PCL chains. We observed similar results [18]. Figure 6f indicates the plot of T$_m$ versus heating rate of PCL. The plot showed an increasing trend. This can be explained on the basis of fast scanning speed.

Hereafter, for further analysis, the PCL synthesized at [M] of 1.5 g was considered for the sake of convenience.

3.2.5 VSM study

The VSM study reveals that after the nanocomposite formation (in solid disc form), the magnetization value was decreased to 21.5 emu/g (Fig. 1i). The decrease in VSM value of Fe$_3$O$_4$–CR end PCL was due to the encapsulation effect (i.e.) the Fe$_3$O$_4$ nanoparticles occupied the free space available between the polymer chains. The VSM study confirmed our prior results that both surface functionalization reaction and nanocomposite formation suddenly reduced the VSM value of Fe$_3$O$_4$ [32].

3.2.6 GPC, FESEM analysis and XRD analysis

In order to confirm the PCL formation GPC measurements were made. The GPC of PCL synthesized at the [M] = 1.50 g is shown in Fig. 7a. The M$_w$, M$_n$ and polydispersity (PD) values were noted as 8417 g/mol, 6119 and 1.37 respectively. The PD value confirmed the absence of crosslinking reactions during the ROP reaction. Figure 7b is the FESEM image of PCL/Fe$_3$O$_4$–CR nanocomposite system
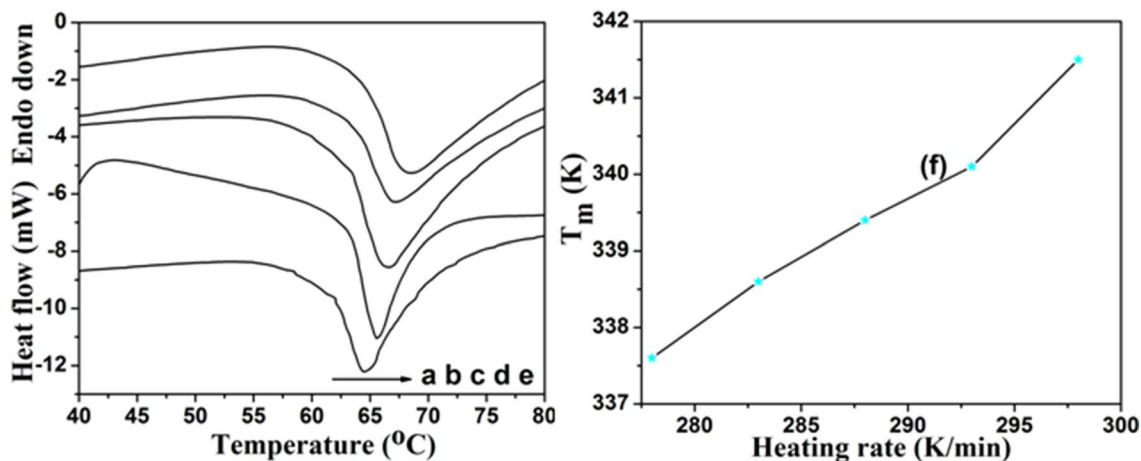

Fig. 6 DSC thermogram of PCL/Fe$_3$O$_4$–CR nanocomposite synthesized at [M] = 1.50 g and at various heating rates of **a** 5 °C/min, **b** 10 °C/min, **c** 15 °C/min, **d** 20 °C/min, **e** 25 °C/min and **f** plot of T$_m$ versus heating rate
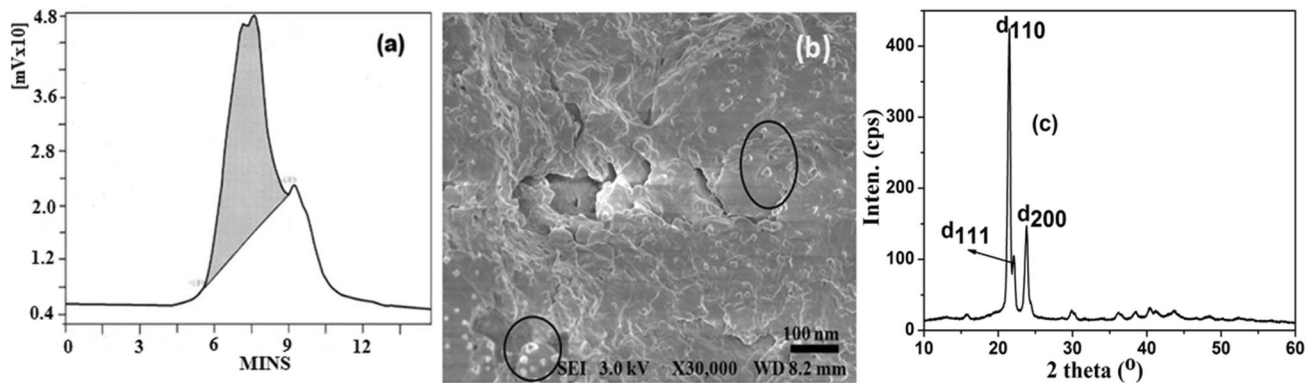
Fig. 7 **a** GPC trace, **b** FESEM image and **c** XRD of the PCL/Fe$_3$O$_4$–CR nanocomposite system synthesized at [M] = 1.50 g

synthesized at [M] = 1.50 g. Here one can see the broken stone like morphology. This is the peculiar surface morphology of the PCL. Some micro voids can also be seen on the surface of PCL. This will help us to load the drug molecules in the bio-medical applications. The Fe$_3$O$_4$ nanoparticles are uniformly distributed on the PCL backbone. Spherical and triangle shaped (marked by a circle) Fe$_3$O$_4$ nanoparticles were present on the surface of the PCL. The size was calculated as 15–20 nm. When compared to the pristine Fe$_3$O$_4$ and its nanohybrid systems, the nanocomposite system exhibited the smallest ferrite size. This can be explained on the basis of the applied thermal energy and the mechanical (agitation) force might help to reduce the size of Fe$_3$O$_4$ [32]. The semi-crystalline nature of the PCL was confirmed by XRD analysis as shown in Fig. 7c. The diffractogram showed crystalline peaks at 21.3°, 22.0° and 23.7° corresponding to d$_{110}$, d$_{111}$ and d$_{200}$ crystalline planes of PCL [33]. The crystalline peaks of ferrite were appeared at 15.8°, 29.9°, 36.3°, 38.4°, 40.3°, 43.7°.

3.3 Non-isothermal degradation kinetics of PCL/Fe$_3$O$_4$–CR nanocomposite system

3.3.1 TGA study

The TGA thermogram of pristine –OH end capped PCL is given in Fig. 8a with a single step degradation process. A major weight loss was noticed at 392.3 °C due to the degradation of PCL backbone [17]. For the sake of comparison, the simple Fe$_3$O$_4$ (0.0085 g) loaded –OH end capped PCL is given in Fig. 8b with a single step degradation process. The major weight loss corresponding to the degradation of PCL backbone occurred at 388.4 °C. Above 450 °C the system exhibited 7.4% weight residue remained. This is corresponding to the loaded Fe$_3$O$_4$ nanoparticles. When compared with the degradation temperature (T$_d$) of pristine PCL with PCL/Fe$_3$O$_4$ nanocomposite system, the later exhibited the lower T$_d$ due to increase in viscosity of the
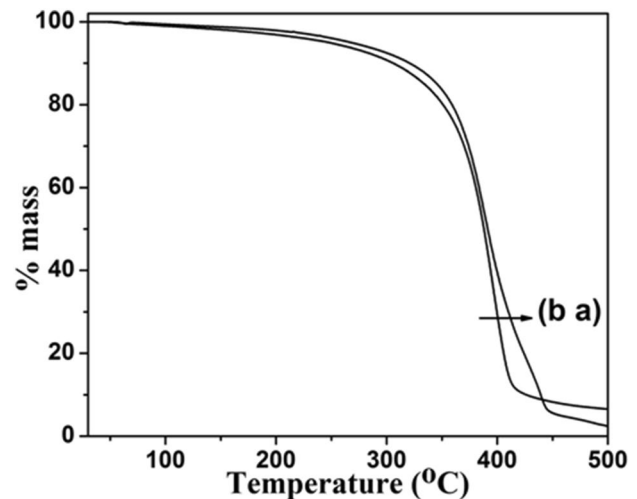

Fig. 8 TGA thermogram of **a** pristine PCL and **b** PCL/Fe$_3$O$_4$ nanocomposite system

reaction medium during its synthesis in the presence of Fe$_3$O$_4$. The PCLs were synthesized in the presence of water as an initiator and SO as a catalyst. This leads to the decrease in M$_w$ of the PCL. Here the main aim of the present research work is to study the non-isothermal degradation kinetics of PCL synthesized in the presence of Fe$_3$O$_4$/CR nanohybrid system.

The third part of the characterization of PCL/Fe$_3$O$_4$–CR nanocomposite system is the non-isothermal degradation kinetic study. The degradation kinetics of PCL was characterized by TGA. PCL synthesized at [M] = 1.50 g was taken. The PCL was subjected to degradation at various heating rates such as 5, 10, 15, 20 and 25 °C/min. The system exhibited a single step degradation process due to the degradation of the PCL backbone with the liberation of CO$_2$ gas (Fig. 9a–e). It was quite interesting to note that, while increasing the heating rate, the degradation temperature of PCL proportionally increased (Fig. 9f). Above
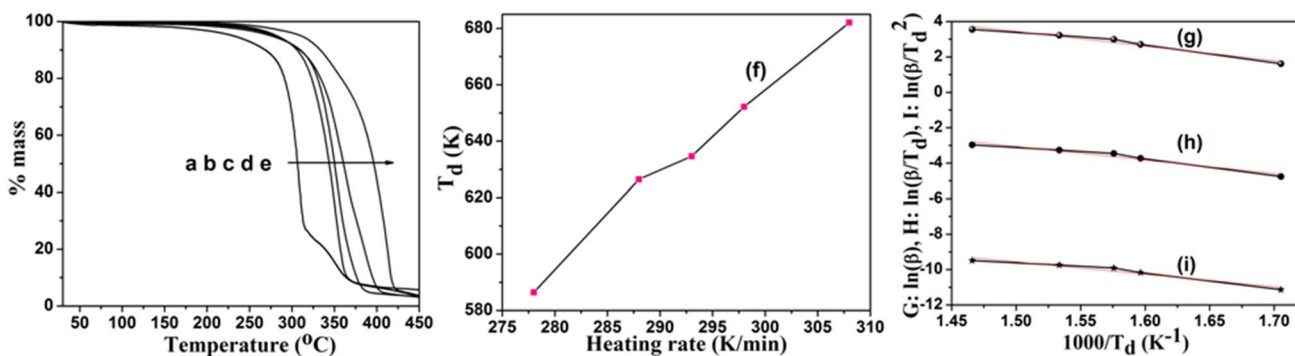
Fig. 9 TGA thermogram of PCL/Fe$_3$O$_4$–CR nanocomposite system synthesized at [M] = 1.50 g recorded at the different heating rates of **a** 5 °C/min, **b** 10 °C/min, **c** 15 °C/min, **d** 20 °C/min, **e** 25 °C/min,

f plot of heating rate versus T$_d$, **g** FWO plot, **h** Auggis–Bennet plot and **i** Kissinger plot
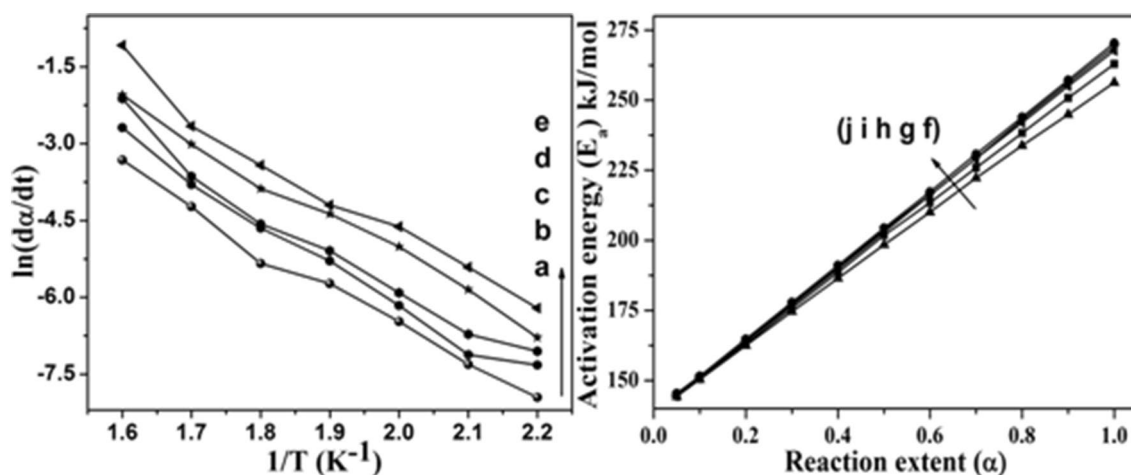

Fig. 10 **a**–**e** Friedman plot, **f**–**j** KAS plot for PCL-Fe$_3$O$_4$–CR nanocomposite system synthesized at [M] = 1.50 g recorded at the different heating rates of **a** 5 °C/min, **b** 10 °C/min, **c** 15 °C/min, **d** 20 °C/min and **e** 25 °C/min

the T$_m$, the chains can move away from each other. While increasing the heating rate, the secondary forces of attraction between the polymer chains were broken and set free to move. In order to find out the energy of activation (E$_a$), for the degradation of the PCL backbone, three models were tried. First the E$_a$ value was determined by the FWO method [34, 35]. In this method, the plot of ln(β) versus 1/T$_d$ (Fig. 9g) was made, from which the E$_a$ and A values were calculated as 158 kJ/mol and 15.8 respectively. β-is the heating rate and T$_d$ is the degradation temperature. The second method was the Auggis and Bennet method. Here the plot of ln(β/T$_d$) versus 1/T$_d$ (Fig. 9h) was drawn with the decreasing trend. The E$_a$ and A values were calculated as 146 kJ/mol and 8.4 respectively. Finally, the Kissinger method was adopted by drawing 1/T$_d$ versus ln(β/T$_d^2$) (Fig. 9i). The plot showed a decreasing trend and from the slope value the E$_a$ value was calculated as 134 kJ/mol. The pre-exponential factor A was calculated from the

intercept of the plot as 0.958. This is in accordance with our earlier results [34]. This degradation kinetics indicated that ~ 150 kJ/mol was required for the degradation of the PCL chains.

3.3.2 Friedman method and KAS method

The ultimate aim of the present investigation is determination of E$_a$ by different methods that include the iso-conversional method too. The E$_a$ for the degradation of PCL was calculated by Friedman method by drawing a plot between ln(dα/dt) versus 1/T (Fig. 10a–e). The α indicates the reaction extent. The plot showed a linear decreasing trend for all the five heating rates. From the slope value of all five heating rates, the E$_a$ value was calculated. While increasing the heating rates, the E$_a$ value was slowly increased. It varied between 143 and 152 kJ/mol. The E$_a$ value for the degradation of PCL was
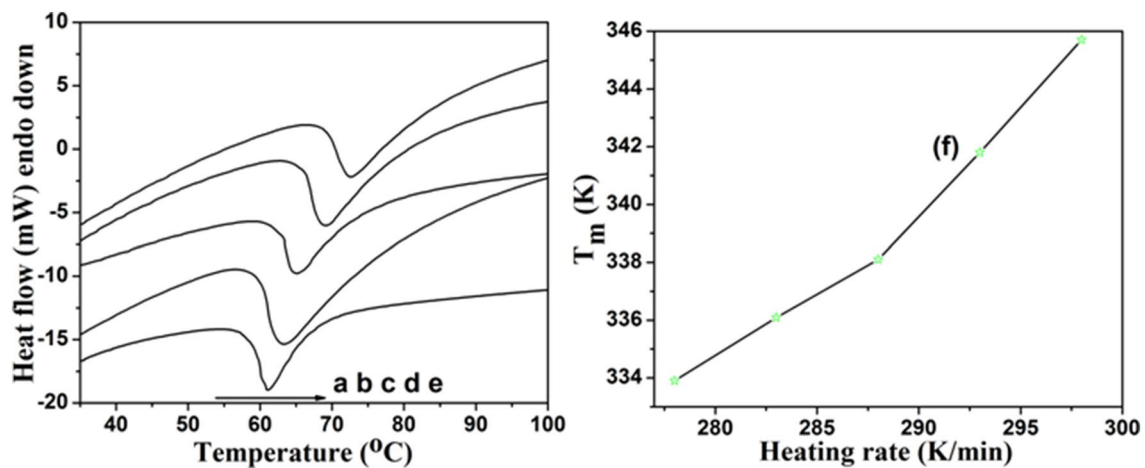
Fig. 11 DSC thermogram of PCL/Fe$_3$O$_4$–MO nanocomposite synthesized at [M] = 1.50 g at various heating rates of **a** 5 °C/min, **b** 10 °C/min, **c** 15 °C/min, **d** 20 °C/min, **e** 25 °C/min and **f** plot of heating rate versus T$_m$

also determined by integral isoconversional method (KAS). The E$_a$ for each heating rate was determined and plotted against the extent of reaction (α) (Fig. 10f–j). It was found that the E$_a$ value linearly increased with the α value. The E$_a$ value varied between 144 and 270 kJ/mol at each heating rate. The linear increase in E$_a$ values were attributed to the rate-limiting step of a random chain scission reaction during the process of heating. This is in accordance with a report by Goswami et al. [36]. The E$_a$ values determined by this method is very nearer to the value determined by the other methods.

3.3.3 DSC study of PCL/Fe$_3$O$_4$–MO nanocomposite system

The DSC thermograms of PCL at the different heating rates are given in Fig. 11a–e. The T$_m$ of the PCL was found to be varying from 62 to 73 °C with increasing heating rate [18]. This is due to the fast scanning of PCL chains. For clear understanding, the plot of heating rate versus T$_m$ is given in Fig. 11f.

3.4 Non-isothermal degradation kinetics of PCL/Fe$_3$O$_4$–MO nanocomposite system

3.4.1 TGA profile

The fourth part of the present investigation was the non-isothermal degradation kinetic study of PCL/Fe$_3$O$_4$–MO nanocomposite system synthesized at [M] = 1.50 g at different heating rates of 5, 10, 15, 20 and 25 °C/min. The influence of MO structure on the thermal degradation behavior of PCL was investigated with the aid of TGA. The PCL sample synthesized at the [M] = 1.50 g was considered. As for the DSC studies, the

sample was heated under air atmosphere at five different heating rates, namely, 5, 10, 15, 20 and 25 °C/min. The TGA thermograms of PCL/Fe$_3$O$_4$–MO nanocomposite system recorded at various heating rates are given in Fig. 12a–e. The system showed a two step degradation process of PCL. The first slow degradation step up to 250 °C was ascribed to the removal of moisture and breaking of linkage between initiator (Fe$_3$O$_4$–MO) and PCL chains. The second major weight loss around 400 °C was attributed to the degradation of PCL backbone. While increasing the heating rates, the T$_d$ value increased proportionally (Fig. 12f). Various kinetic models are used in order to find out the E$_a$ value for the degradation of PCL chains. For this purpose, FWO plot (Fig. 12g), Auggis–Bennet plot (Fig. 12h) and Kissinger plot (Fig. 12i) were drawn and the E$_a$ values were calculated as 218.09, 196.45 and 174.72 kJ/mol, respectively. The Ba thioglycolate end capped PCL consumed nearly 120 kJ/mol for its own degradation under air atmosphere [37]. The Fe$_3$O$_4$-dye end capped PCL consumed lower amount of thermal energy for its degradation. This indicated that the E$_a$ for the T$_d$ of PCL depended on the nature of end capping agent as well as the molecular weight of PCL. When compared with the CR based system, the present MO based system consumed higher amounts of thermal energy for the degradation of the PCL chains. This proved that the structure of dye (nature of initiating functional group and other functional groups available) played a vital role on the thermal property of PCL.
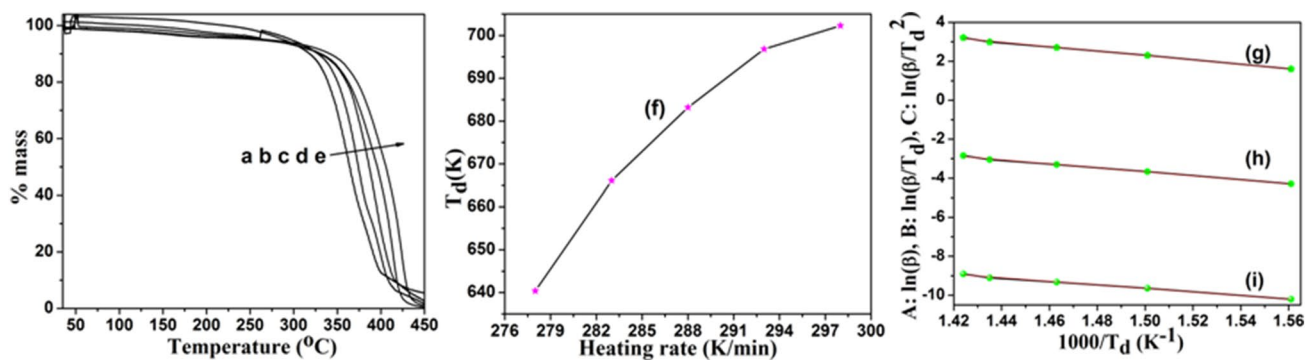
Fig. 12 TGA thermogram of PCL/Fe$_3$O$_4$–MO nanocomposite system synthesized at [M] = 1.5 g recorded at the different heating rates of **a** 5 °C/min, **b** 10 °C/min, **c** 15 °C/min, **d** 20 °C/min, **e** 25 °C/min, **f** plot of heating rate versus T$_d$, **g** FWO plot, **h** Auggis–Bennet plot and **i** Kissinger plot
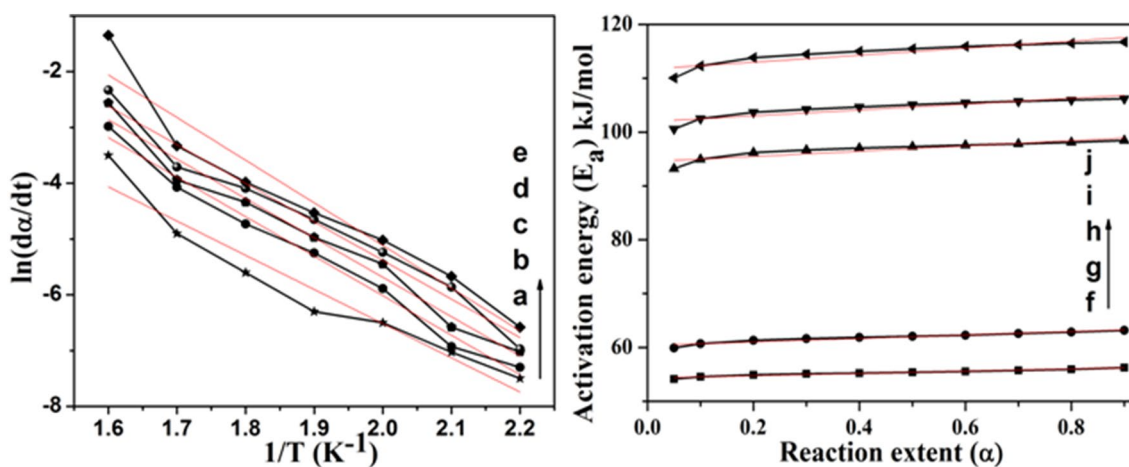

Fig. 13 **a**–**e** Friedman plot, **f-j** KAS plot for PCL-Fe$_3$O$_4$–MO nanocomposite system synthesized at [M] = 1.50 g recorded at the different heating rates of **a** 5 °C/min, **b** 10 °C/min, **c** 15 °C/min, **d** 20 °C/min and **e** 25 °C/min

3.4.2 Friedman method and KAS method

For the present system the E$_a$ value were also determined by the Friedman method by plotting 1/T versus ln(dα/dt) (Fig. 13a–e). As usual, the plot showed a decreasing trend with increasing temperature. The E$_a$ value varied between 117 and 146 kJ/mol. The E$_a$ values for the degradation of PCL were also determined by the KAS method. Figure 13f–j indicates the plot of reaction extent (α) versus activation energy. The activation energy varied between 54 and 117 kJ/mol. With increasing the reaction extent, the E$_a$ value very slowly increased. While increasing the heating rate, the E$_a$ value increased considerably. In the case of the PCL-Fe$_3$O$_4$–CR system, while increasing the reaction extent, the E$_a$ value was increased in a linear manner for any given heating rate. In comparison we conclude that the degradation kinetics of PCL can be altered by the end group attached to the PCL chain end.

4 Summary

From the above study the niche points are presented here as summary. The red shift in the UV–visible spectrum of CR dye confirmed the nanohybrid formation with Fe$_3$O$_4$. The reduction in VSM value of Fe$_3$O$_4$ nanoparticle also confirmed the nanohybrid formation. The FTIR relative intensity of [C=O/C–H] was found to be increased while increasing the [M]. This is due to the decrease in initiating species concentration. While increasing the weight of CL, the absorbance value was found to be reduced. The same results were observed in the case of FES while increasing the weight of CL. The T$_m$ value of PCL increased while increasing the [M] due to the availability of more number of monomeric units. The degradation temperature of PCL was increased while increasing the heating rates. The E$_a$ value was determined from the Kissinger plot as 134.25 kJ/

mol for the degradation of PCL backbone in PCL/Fe$_3$O$_4$–CR system.

Compliance with ethical standards

Conflict of interest The authors declare that they have no conflict of interest.

References

1. Murugesan A, Meenarathi B, Kannammal L, Palanikumar S, Anbarasan R (2014) Synthesis, characterization and drug delivery activity of poly(anthranilicacid) based triblock copolymer. Synth Met 189:143–151
2. Kannammal L, Palanikumar L, Meenarathi B, Anbarasan R (2014) Synthesis, characterization and band gap energy of poly(ε-caprolactone)/Sr-MSA nanocomposite. J Phys D Appl Phys 47:1–10
3. Sivabalan A, Harihara Subramani R, Meenarathi B, Anbarasan R (2014) Chemical initiators initiated ring opening polymerization of ε-caprolactone. Int J Sci Res Eng Tech 1:9–14
4. Oshimura M, Takasu A (2010) Controlled ring opening polymerization of ε-caprolactone catalyzed by rare earth perfluoroalkanesulfonates and perfluoroalkanesulfonimides. Macromolecules 43:2283–2290
5. Yan Y, Zhang Y, Xiao Y, Zhang Y, Lang M (2010) Novel poly(ε-caprolactone)s bearing amino groups: synthesis, characterization and biotinylation. React Funct Polym 70:400–407
6. Hemmati K, Masoumi A, Ghaemy M (2015) pH responsive tragacanth gum and poly(methyl methacrylate-co-maleicanhydride)-g-poly(caprolactone) network microgel for invitro quercetin release. Polymer 59:49–56
7. Yang L, Li J, Jin Y, Li M, Gu Z (2015) In vitro enzymatic degradation of the cross-linked poly(ε-caprolactone) implants. Polym Degrad Stab 112:10–19
8. Cao H, Feng Y, Wang H, Zhang L, Khan M, Guo J (2011) Synthesis of depsipeptides from L-amino acids and lactones. Front Chem Sci Eng 5:409–415
9. Oledzka E, Narine S-S (2011) Organic acids catalyzed polymerization of ε-caprolactone: synthesis and characterization. J Appl Polym Sci 119:1873–1882
10. Limwanich W, Khunmanee S, Kungwan N, Punyodom W, Meepowpan M (2015) Effect of tributyltin alkoxides chain length on the ring-opening polymerization of ε-caprolactone: kinetics studies by non-isothermal DSC. Thermochim Acta 599:1–7
11. Koopmans C, Iannelli M, Kerep P, Klink M, Schmitz S, Sinnwell S, Ritter H (2006) Microwave assisted polymer chemistry: heck reaction, transesterification, Baeyer–Villiger oxidation, oxazoline polymerization, acrylamides, and porous materials. Tetrahedron 62:4709–4714
12. Wang G-S, Wei Z-Y, Sang L, Chen G-Y, Zhang W-X, Dong X-F (2013) Morphology, crystallization and mechanical properties of poly(ε-caprolactone)/graphene oxide nanocomposites. Chin J Polym Sci 31:1148–1160
13. Contreras J-M, Medina D, Carrasquero F-L, Contreras R-R (2013) Ring opening polymerization of ε-caprolactone initiated by samarium acetate. J Polym Res 20:244–250
14. Hao J, Granowski P-C, Stefan M-C (2012) Zinc undecylenate catalyst for the ring opening polymerization of caprolactone monomers. Macromol Rapid Commun 33:1294–1299
15. Agathian K, Meenarathi B, Kannammal L, Anbarasan R (2013) Luminol initiated ring opening polymerization of caprolactone. Ind J Sci 5:37–40
16. Meenarathi B, Chen H-H, Chen P-H, Anbarasan R (2013) Near infrared dye functionalized MWCNT as an effective initiator for the ring opening polymerization of ε-caprolactone. J Polym Res 20:118–130
17. Meenarathi B, Kannammal L, Palanikumar S, Anbarasan R (2014) Synthesis and characterizations of Fe$_3$O$_4$-acid fuchsin tagged poly(ε-caprolactone) nanocomposites. Mater Res Exp 1:1–17
18. Meenarathi B, Palanikumar S, Kannammal L, Anbarasan R (2015) Synthesis, characterization and catalytic activity of Ag-acidfuchsin nanohybrid system towards the ring opening polymerization of ε-caprolactone. Spectrochim Acta Part A Mol Biomol Spectosc 135:93–100
19. Meenarathi B, Chen H-H, Chen H-H, Anbarasan R (2014) Synthesis and characterization of fluorescent bio-degradable poly(ε-caprolactone). Int J Plast Technol 18:135–145
20. Meenarathi B, Palanikumar S, Kannammal L, Anbarasan R (2016) Synthesis, characterization and drug release activity of poly(ε-caprolactone)/Fe$_3$O$_4$–alizarinred nanocomposites. Nanocomposites 2:98–107
21. Chizari M, Bayat Y (2018) Synthesis and kinetic study of a PCL-GAP-PCL triblock copolymer. Cent Eur J Enererg Mater 15:243–257
22. Marquez Y, Franco L, Puiggali J (2012) Thermal degradation studies of poly(trimethylenecarbonate) blends with either poly(lactide) or poly(caprolactone). Thermochim Acta 550:65–75
23. Aoyagi Y, Yamashita K, Doi Y (2002) Thermal degradation of poly(hydroxybutyrate), poly(caprolactone) and poly(lactide). Polym Degrad Stab 76:53–59
24. Su T-T, Jiang H, Gong H (2008) Thermal stabilities and thermal degradation kinetics of poly(caprolactone). Polym Plast Technol Eng 47:398–403
25. Sivalingam G, Karthik R, Madras G (2003) Kinetics of thermal degradation of poly(ε-caprolactone). J Anal Appl Pyrol 70:631–647
26. Palanikumar S, Siva P, Meenarathi B, Anbarasan R (2014) Effect of F$_{e3O4}$ on the sedimentation and structure–property relationship of starch under different pHs. Int J Biol Macromol 67:91–98
27. Palanikumar S, Kannammal L, Meenarathi B, Anbarasan R (2014) Effect of folic acid decorated magnetic fluorescent nanoparticles on the sedimentation of starch molecules. Int Nano Lett 4:104–113
28. Kailash S, Meenarathi B, Kannammal L, Palanikumar S, Anbarasan R (2015) Synthesis, characterization, drug delivery and splinting activity of folicacid bridged poly(ε-caprolactone-co-tetrahydrofuran). Int J Polym Mater Polym Biomater 64:620–627
29. Kohila V, Sribala G, Meenarathi B, Anbarasan R (2014) Synthesis and spectral characterizations of poly(congored) grafted silk fibre-A kinetic approach. Ind J Fibre Text Res 39:172–179
30. Ansari M, Kordestani S-S, Rezaei M-H, Moosavi A-A, Movahedi M (2015) Synthesis and characterization of acylated polycaprolactone (PCL) nanospheres and investigation of their influence on aggregation of amyloid proteins. J Macromol Sci Part B Phys 54:71–80
31. Omrania M-M, Kiaie N, Ansari M, Kordestani S-S (2016) Enhanced protein adsorption, cell attachment and neural differentiation

with the help of amine functionalized poly(caprolactone) scaffolds. J Macromol Sci Part B Phys 55:617–626

32. Palanikumar S, Meenarathi B, Kannammal L, Anbarasan R (2015) Synthesis, characterization and catalytic activity of furosemide-functionalized ferrite on the sedimentation behavior of starch. Appl Nanosci 5:83–91

33. Kannammal L, Meenarathi B, Palanikumar S, Udhayaranjan S, Premkumar H, Anbarasan R (2014) Synthesis and characterization of poly(ascorbic acid) by ring opening polymerization. J Sci 4:66–73

34. Jancirani A, Kohila V, Meenarathi B, Anbarasan R (2016) Synthesis, characterisation and non-isothermal degradation kinetics of novel poly(monoethyleneglycol dimethacrylate-co-4-aminobenzoate). Bull Mater Sci 39:1725–1733

35. Parthasarathi V, Dhanalakshmi V, Anbarasan R (2015) Thermal studies on benzamide and benzanilide grafted LDPE. J Therm Anal Calorim 119:73–84

36. Goswami A, Sivalingam G, Umarji A, Madras G (2012) Thermal degradation kinetics of poly(trimethylol propane triacrylate)/poly(hexanediol diacrylate) interpenetrating polymer network. Thermochim Acta 547:53–61

37. Mahalakshmi S, Alagesan T, Parthasarathy V, Tung KL, Anbarasan R (2019) Non-isothermal crystallization kinetics and degradation kinetics studies on barium thioglycolate end capped poly(ε-caprolactone). J Therm Anal Calorim 135:3129–3140

Publisher's Note Springer Nature remains neutral with regard to jurisdictional claims in published maps and institutional affiliations.